PCCP

ROYAL SOCIETY OF CHEMISTRY

PAPER

View Article Online
View Journal | View Issue

Cite this: *Phys. Chem. Chem. Phys.*, 2025, **27**, 16636

Machine learning based prediction of MnO_2 cathode discharge capacity for high-performance zinc-ion batteries†

Nure Alam Chowdhury,[ab] Leaford Nathan Adebayo Henderson,[ab] Samin Yaser,[c] Olusola Pelumi Oyeku,[ab] Maydenee Maydur Tresa,[ab] Chandra Kundu[d] and Jayan Thomas*[abe]

Received 28th March 2025,
Accepted 3rd July 2025

DOI: 10.1039/d5cp01218j

rsc.li/pccp

Zinc-ion batteries (ZIBs) are considered as a cheaper, non-toxic and safer alternative to lithium-ion batteries (LIBs). Manganese dioxide (MnO_2) is one of the most viable cathode materials for aqueous electrolyte based ZIBs. The addition of different dopants in the MnO_2 cathode material can significantly change its physical properties and electrochemical performance in ZIBs. In this study, we collected about 603 papers from which we selected 57 ZIB published papers related to doped MnO_2 as a cathode material. The dataset consists of a total of eleven features (ten input features and one target) in which six features are related to battery properties and five features are related to the elemental properties of the dopants. The Pearson correlation plot is considered to investigate the correlation between different features, and it is observed that the electronegativity and first-ionization energy of the dopant have a positive relation with discharge capacity (DC). Both classification and regression treatment are applied to our dataset using different machine learning models such as XGBoost, random forest (RF), and *K*-nearest Neighbors. The RF model can classify DC with an accuracy of 0.72 into three predefined grades. In the regression analysis, the XGBoost model can predict DC with an R^2 value of 0.92. Finally, the findings of this study can be utilized to predict the performance of doped MnO_2 before synthesizing it in the laboratory.

1. Introduction

The development of technology has rigorously changed the dynamics of our life. There are two ways by which one can categorize modern technology: one is the system, and the other is energy which is required to run the system. For example, the mobile phone is a system, and to run the mobile phone, we do need energy. Even though exponential progress has been made in the development of the system, a similar momentum cannot be found in the field of energy storage. Lithium-ion batteries (LIBs) have been considered as the appropriate source of energy for small-scale applications.[1–3] But due to the limited resources of lithium, it is time to think about a potential alternative to LIBs. Zinc-ion batteries (ZIBs) can be considered as a potential alternative to LIBs due to their availability,[4–6] high theoretical specific capacity (*i.e.*, 820 mAh g^{-1}),[7–9] non-flammability,[10–12] non-toxicity,[13] easy processability, and long shelf-life.[14]

ZIBs encounter several problems associated with cathode materials. The most promising candidates for cathode materials for ZIBs are manganese-based oxides,[15–17] vanadium-based oxides,[18–20] Prussian blue analogues,[21–23] *etc.* One of the leading candidates among these is manganese dioxide (MnO_2) due to its good voltage, high discharge capacity, and ease of synthesis with different crystal structures, *viz.*, α-MnO_2,[24] β-MnO_2,[25] γ-MnO_2,[26] ε-MnO_2,[27] λ-MnO_2,[28] and layered structures.[29–31] Different crystal structures exhibit different tunnel or layer spacings that can modify the ionic intercalation/de-intercalation behavior of the material and potentially lead to different specific capacities. However, the major problems associated with the MnO_2 cathode include low electronic conductivity (10^{-5} S cm^{-1} to 10^{-6} S cm^{-1}),[32] and the other is the Jahn–Teller effect.[33–35] The structure of MnO_2 experiences a phase transition during successive charging/discharging cycles, and with time, this structural change can degrade the MnO_2 cathode material.[36] Dopants can assist MnO_2 in stabilizing its crystal

[a] *Nanoscience and Technology Center, University of Central Florida, Orlando, FL 32826, USA. E-mail: Jayan.Thomas@ucf.edu*
[b] *Department of Materials Science and Engineering, University of Central Florida, Orlando, FL 32816, USA*
[c] *College of Engineering and Computer Science, University of Central Florida, Orlando, FL 32816, USA*
[d] *Department of Statistics and Data Science, University of Central Florida, Orlando, FL 32816, USA*
[e] *CREOL, The College of Optics and Photonics, University of Central Florida, Orlando, FL 32816, USA*

† Electronic supplementary information (ESI) available. See DOI: https://doi.org/10.1039/d5cp01218j

structure for a long time and can improve the performance profile of MnO_2. The presence of Mo in γ-MnO_2 shows superior rate capabilities and cycling stability, and enhances the diffusion kinetics of ions and electrons.[36] When aluminum (Al) is doped into birnessite-type δ-MnO_2, it can be seen that Al can prevent a structural collapse by minimizing the growth of microcracks during charging and discharging.[37] Experimental observation has confirmed that the doping of magnesium (Mg) in tunnel-type α-MnO_2 can minimize the reaction resistance and diffusion, and can improve the ion diffusion coefficient and also boost the stability of the crystal structure.[38]

Machine learning (ML), which is a modern mathematical framework, can be used to read, understand, and predict the complex internal connection of different data points.[39–41] With the development of advanced algorithms, ML models (MLMs) can be used to explore the cryptic relationships of colossal data within a short period of time; however, the exact relationships cannot be discovered using traditional trial–error methods.[39–41] MLMs have been considered in designing battery materials, analyzing the chemical compositions of the anode, cathode, and separator, optimizing the battery performance, and predicting the health of the battery before fabrication and testing.[42–45] MLMs can suggest new super-ion conductors and can predict the performance of solid electrolytes 10^9 times faster compared to density functional theory calculations with a mean absolute error of 0.25 eV.[46] A manually curated dataset has been considered for applying MLMs to predict the initial discharge capacity (DC) and that at end of the 20th cycle.[47] In that case, MLMs can predict the initial DC with a value of R^2 = 0.53 and that at the end of 20th cycle with R^2 = 0.54.[47] The existence of different dopants can change the electrochemical properties of the lithium, nickel, cobalt, and manganese in various cathode materials for LIBs.[48] MLMs have been applied to study the relation between the DC and the structural and elemental features of different dopants. The gradient boost model can predict the initial (50th cycle) DC with R^2 = 0.76 (R^2 = 0.64).[48] The ML approach can differentiate the impact of different physical properties associated with dopants on metal-oxide based photoelectric materials.[49] ML is also used in the field of supercapacitors.[50] The multilayered perception and random forest (RF) models have been used to classify the specific capacitance of four pre-defined grades. Recently, four ML classifier models were considered to classify the DC of TiO_2 anode materials in the presence of fourteen dopants for LIBs.[51] For this purpose, 316 samples and eleven features associated with different published papers were considered. The gradient boosting model achieved an accuracy of 0.79 and a specificity of 0.90 for classification.[51]

Even though considerable effort has been invested in predicting the effect of dopants in many important LIB cathodes, no attempt has been made to predict the DC of the MnO_2 cathode material for ZIBs with different dopants by applying the MLMs. The aim of the present work is to collect data associated with dopants which can improve the performance of the MnO_2 cathode material for ZIBs from 57 published papers. We will apply both classification and regression treatment to our dataset by considering different MLMs, *viz.*, RF,[51] *K*-nearest neighbors (KNN),[52] and XGBoost[53] to classify and predict the DC of doped MnO_2.

2. Methods

2.1. Data collection and feature analysis

The blueprint of our work is shown in Fig. 1. Initially, we fix our goal to classify and predict the DC of MnO_2 by using different MLMs. For this purpose, we collect the data, and then observe correlations between different features, extract the features, train and test different MLMs, and classify and predict the DC of MnO_2. In the ML approach, data collection and preprocessing are the most important steps. In our case, we have carefully followed the following protocols for collecting our datasets: (i) first, the publications related to ZIBs were searched and around 603 papers were collected; (ii) the publications which used MnO_2 as the cathode material were considered in the next step; and (iii) the articles which used only one dopant were selected. After following these steps, we were able to manage to select 57 articles, which were related to the single-dopant MnO_2 cathode material for ZIBs. The dataset contains a total of 25 different dopants (see Fig. S1, ESI†). We considered a total of 11 features, which include 6 publication results and 5 elemental properties (see Table 1).

We employed the Pearson correlation matrix (PCM) to examine relevant associations among features. The PCM quantifies pairwise linear relationships between variables and enables visual interpretation through a heatmap (see Fig. 2). Among the features, there is a moderate relationship that can be observed between the current and DC (*i.e.*, $r = -0.5$), reporting that the DC decreases with the value of current. This negative correlation observed between DC and current likely

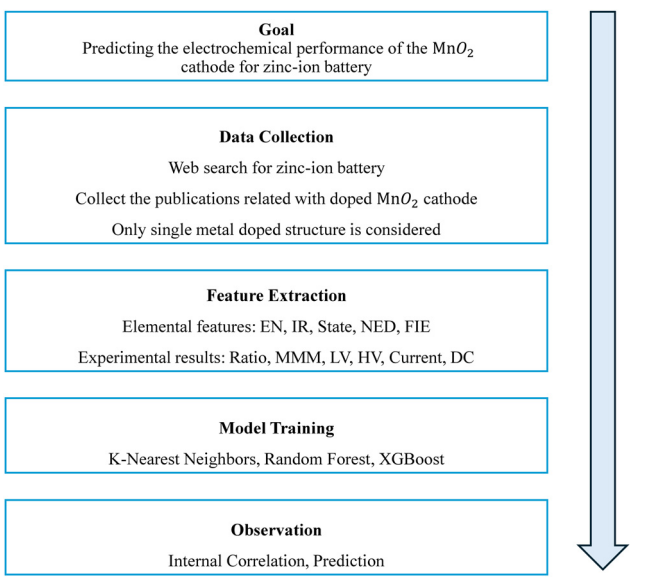

Fig. 1 The workflow of the current work. Initially, the goal of our article is presented, and then data collection, feature extraction, model training and finally feature importance are discussed.

Table 1 Covariate and response variables and their related abbreviations

Covariates			
Elemental features		Publication results	
Name	Abbreviation	Name	Abbreviation
Electronegativity of doped elements	EN	Atom ratio of dopant and Mn	Ratio
Ionic radius (in pm) of the dopant	IR	Molar mass of the molecule	MMM
State of the dopant	State	Lowest voltage during charging and discharging (V)	LV
Number of electrons of the dopant	NED	Highest voltage during charging and discharging (V)	HV
First ionization energy (in kJ mol^{-1})	FIE	Current density (A g^{-1})	Current

Response variable	
Name	Abbreviation
Discharge capacity (mAh g^{-1})	DC

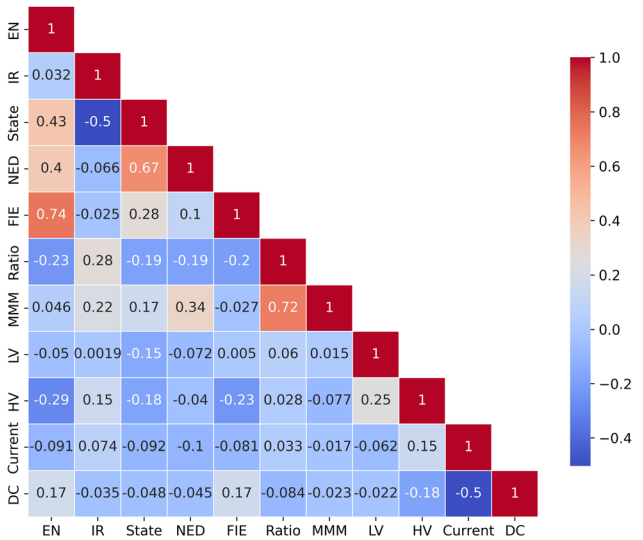

Fig. 2 Pearson coefficient correlation for different elemental and experimental features.

reflects the effect of polarization within the battery, a well-known phenomenon noticed predominantly at high charging/discharging rates.[54] On the other hand, a weak positive correlation (*i.e.*, r = 0.17) can be observed between EN and DC, manifesting that higher EN is weakly associated with increased DC for ZIBs. Similarly, the weak positive correlation (*i.e.*, r = 0.17) between FIE and DC suggests that higher FIE values may be modestly increasing the DC of the ZIBs. This could be explained *via* the mechanism of dopant stabilization of the crystal structure of MnO_2 described earlier. Due to the increased local charge in the vicinity of the dopant ions, which is strongly correlated with the actual electronegativity of the ion itself, the electrical conductivity of the bulk material is increased, which would be expected to also improve DC.[55] This effect is also expected to improve the stability of the crystal structure due to the suppressed Jahn–Teller distortion; so, although battery cycle life was not a feature captured in this study, it may be worth including in a future investigation. Of note, DC is expected to show a similar trend to both EN and FIE, since both are correlated with the attraction exerted on the outer electrons of the dopant ions by the nucleus; hence, dopants with higher electronegativities are harder to ionize and have larger associated FIE.

Strong inter-feature correlation can be observed for different variables, for example, FIE and the EN (*i.e.*, r = 0.74). The ratio of dopant to Mn and MMM has a high positive correlation (*i.e.*, r = 0.72), indicating that the existence of different ratios can determine the MMM. The presence of highly correlated variables in the dataset can provide us with a detailed picture of the interaction of the data points and can guide us to determine which variables are important to change the physical properties of the system. Features with low correlations may not provide essential information for the linear treatment of the dataset but could be important for the nonlinear predictive MLMs. Overall, the correlation matrix can provide a primary valuable insight regarding the feature interdependence and can guide us in incorporating different MLMs. The histogram for different features can be seen in Fig. S2–S4 (ESI†).

2.2. Model training

The MLMs were trained by using Python and its supporting libraries (*viz.*, pandas, matplotlib, Optuna, scikit-learn, XGBoost, *etc.*). We have considered both classification and regression approaches for our dataset. For classification, we split the DC values at the 33.33rd and 66.67th percentiles to create three equally sized grades: (a) grade 0: DC values $<$ 166.65 mAh g^{-1}; (b) grade 1: 166.65 mAh g^{-1} $\leq$ DC values $<$ 248 mAh g^{-1}; and (c) grade 2: DC values $\geq$ 248 mAh g^{-1} (see Fig. 3).

We have tested three different models, *viz.*, KNN, XGBoost, and RF on the dataset. Furthermore, we have built regression models to predict the DC values from given features. For regression purposes, we have utilized KNN, RF, and XGBoost. The dataset was randomly shuffled and split: 15% for the holdout test (*i.e.*, 90 samples) and 85% for training (*i.e.*, 510 samples). The training was done following stratified 10-fold cross-validation, while Bayesian optimization[56] was used for hyper-parameter tuning for individual models. The dataset and code for this article can be found at the following GitHub link: **https://tinyurl.com/396jsa4t**.

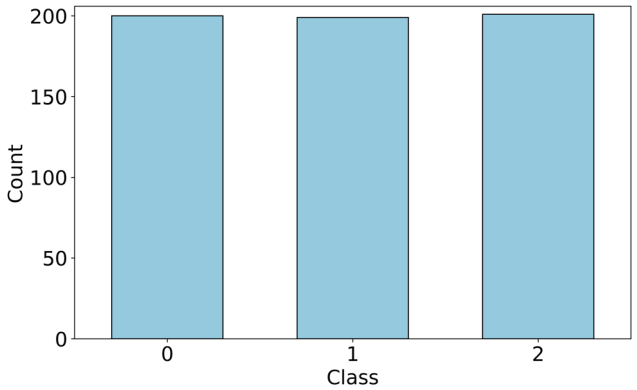

Fig. 3 The bar chart illustrates the distribution of samples across three predefined grades based on DC values. This classification was used to evaluate the performance of different MLMs applied to the dataset.

3. Results and discussion

3.1. Performance evaluation of the MLMs on the classification task

The performance associated with different MLMs is evaluated using four key classification metrics: accuracy, precision, recall, and specificity. The comparison of performance can be seen in Table 2. KNN correctly predicts 69% of the total cases, reflecting a moderate level of predictive capability. Its precision of 0.68 indicates that 68% of the instances labeled as positive are correct, showing a reasonable, though not strong, ability to minimize false positives. The recall, also at 0.68, reveals that the model correctly identifies 68% of all true positive cases, meaning that it misses nearly a third of them. Specificity stands at 0.68, suggesting that the model performs somewhat better at correctly identifying negative cases. This indicates that KNN struggles more than the other models in accurately identifying positive instances.

XGBoost demonstrates consistent and balanced performance across all metrics, achieving a score of 0.70 for accuracy, precision, recall, and specificity. This uniformity suggests that XGBoost performs equally well in identifying both positive and negative cases, while maintaining a good balance between correctly predicting true positives and avoiding false positives. On the other hand, RF outperforms XGBoost across all metrics, with an accuracy of 0.72, a precision of 0.74, a recall of 0.72, and a specificity of 0.72. These higher scores indicate that RF is more effective overall, correctly predicting a larger proportion of both positive and negative cases. Its slightly higher recall and specificity also suggest better reliability in handling grades. While both models are consistent and reliable, RF offers superior predictive performance, making it the more robust option in this comparison. It may be noted that the confusion matrix and the ROC curve for different MLMs can be seen in Fig. S5 and S6 (ESI†).

3.2. Performance evaluation of the MLMs on the regression task

A comparison of performance associated with three different MLMs, *viz.*, KNN, RF, and XGBoost, can be observed in Table 3. The MLM performance can be evaluated *via* four key parameters: R^2, adjusted R^2, root mean square error (RMSE), and mean absolute error (MAE) which can determine the capabilities for generalized implication and robustness to prediction errors.

The KNN model shows strong performance of the training data, with an R^2 of 0.97 and very low error values (a RMSE of 12.99 mAh g^{-1} and a MAE of 4.27 mAh g^{-1}), indicating an excellent fit. However, its performance drops noticeably on the test set, where R^2 decreases to 0.84, and the error values increase significantly (a RMSE of 33.70 mAh g^{-1} and a MAE of 23.91 mAh g^{-1}). This gap between training and testing results suggests that the KNN model captures noise in the training data and fails to generalize well to unseen data.

When comparing RF and XGBoost, both models show good generalization, but XGBoost clearly performs better overall. While RF achieves an R^2 of 0.91 on the training set and 0.86 on the test set, XGBoost posts higher values with an R^2 of 0.97 during training and 0.92 in testing. XGBoost also records lower error metrics across the board, especially on the test set, where its RMSE (24.39 mAh g^{-1}) and MAE (16.23 mAh g^{-1}) outperform RF's RMSE (31.64 mAh g^{-1}) and MAE (23.81 mAh g^{-1}). These results indicate that XGBoost not only fits the training data well but also generalizes more effectively, making it the more accurate and reliable model in comparison. From the perspective of ZIB research, these findings associated with different MLMs can be applied to determine the DC of the doped MnO_2 according to the different related experimental and elemental features before synthesizing the materials in the laboratory. In this context, XGBoost would be the optimal choice for designing the doped MnO_2. The comparison of actual *vs.* predicted DC (mAh g^{-1}) using three different regression models can be seen in Fig. S7 (ESI†).

3.3. Feature importance analysis

The analysis of feature importance serves as a fundamental aspect of applying MLMs to complex systems, offering a clear understanding of the model's decision-making process and providing a valuable direction for future development. Fig. 4 represents the SHAP summary by illustrating the impact of different elemental features and publication results on the

Table 2 Comparison of accuracy, precision, recall, and specificity of different MLMs

MLMs	Accuracy	Precision	Recall	Specificity
KNN	0.69	0.68	0.68	0.68
XGBoost	0.70	0.70	0.70	0.70
RF	0.72	0.74	0.72	0.72

Table 3 Comparisons of R^2, RMSE and MAE values for different MLMs

	Train				Test			
MLMs	R^2	Adjusted R^2	RMSE	MAE	R^2	Adjusted R^2	RMSE	MAE
KNN	0.97	0.97	12.99	4.27	0.84	0.82	33.70	23.91
RF	0.91	0.91	25.56	17.35	0.86	0.84	31.64	23.81
XGBoost	0.97	0.96	15.47	9.38	0.92	0.91	24.39	16.23

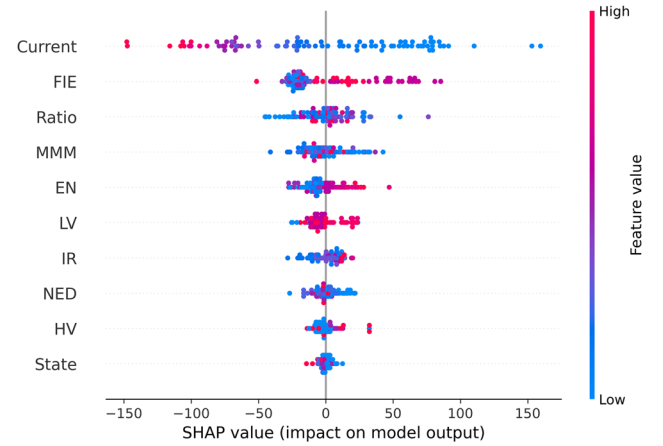

Fig. 4 SHAP summary plot illustrating the importance of different features and the associated direction of influence in predicting DC. The rank of the features has been addressed according to their contribution to the XGBoost regression model.

XGBoost regression model while predicting the DC of MnO_2 in the presence of different dopants. The vertical axis lists the features in descending order of importance, while the horizontal axis shows the SHAP value (impact on the model output), and each point represents a data sample. The color of the points represents the feature value: red (blue) indicates high (low) feature values. Features at the top, such as "Current", have the maximum influence on predictions, while features lower down, like HV and "State", have a lower impact. For instance, for "Current", high values (red points) are associated with negative SHAP values, indicating that higher current decreases DC; conversely, low current (blue points) tends to increase DC. Features like FIE show a substantial influence, with a broader range of SHAP values, indicating their contribution to both increasing and decreasing discharge capacity predictions, even though a cluster can be seen in the negative SHAP values. The ratio and MMM demonstrate a similar trend, where the impact varies depending on the feature value.

EN exhibits a bifurcated effect, where both high and low values influence DC in varying directions, indicating complex interactions. IR shows an intermediate contribution to the decision making of the DC of Zn-ion batteries. In contrast, features like "State" exhibit more clustered SHAP values close to zero, signifying a minimal effect on the output. From a practical standpoint, the XGBoost model effectively learns from the data, handles non-linear effects, and captures meaningful relationships among features, while mitigating over-fitting of the data. The partial-dependence plots in Fig. S8 (ESI†) illustrate its ability to model the non-linear patterns. We calculated the SHAP values using TreeSHAP,[57,58] which inherently accounts for feature dependencies as captured by the model's structure and can be interpreted as interventional Shapley values.[59] However, it is important to note that TreeSHAP primarily addresses dependencies learned by the model and may still misestimate contributions if strong correlations are not explicitly reflected in the tree splits.[60] Overall, this SHAP analysis confirms that the XGBoost model's predictions are driven by features with clear physical and electrochemical significance, enhancing both the model's reliability and interpretability. The outcomes of Fig. 4 are essential to understanding the underlying factors to determine DC and can guide the selection of the features for designing new doped MnO_2.

3.4. Cohort analysis: alkali *versus* transition metals

In Fig. 5, we compared the SHAP-value summaries for two distinct cohorts: (a) alkali metals (Ca, Na, K, Li, and Mg) and (b) transition metals (Mo, Cr, V, Ti, Zn, Cu, Fe, Co, Ag, and Ni). The mean SHAP values for each feature in our XGBoost model on the test set highlight their mostly inverse contributions to distinguishing these two groups. The bar chart presents the average impact of each feature on model's prediction. Bars extending to the left (negative values) indicate features that contribute to lowering the predicted output, whereas bars to the right (positive values) increase it. Each bar is divided into two patterns representing different element types: alkali metals (solid fill) and transition metals (diagonal stripes), with the number of instances for each group shown in brackets in the legend. According to the SHAP analysis, "Current" exhibits the strongest and most contrasting effect on model output among all features. In the alkali group, "Current" has a strongly negative mean SHAP value (−26.33), indicating that higher current levels are responsible for the decrease in predicted DC. In contrast, in the transition group, "Current" shows a positive mean SHAP value (+16.32), implying that higher current contributes to an increase in the predicted DC. FIE shows a similar polarity reversal. For the alkali group, FIE has a mean SHAP value of around −15.89. So, FIE tends to reduce the predicted DC. On the other hand, for the transition group, FIE has a mean SHAP value of around +21.47. So, in

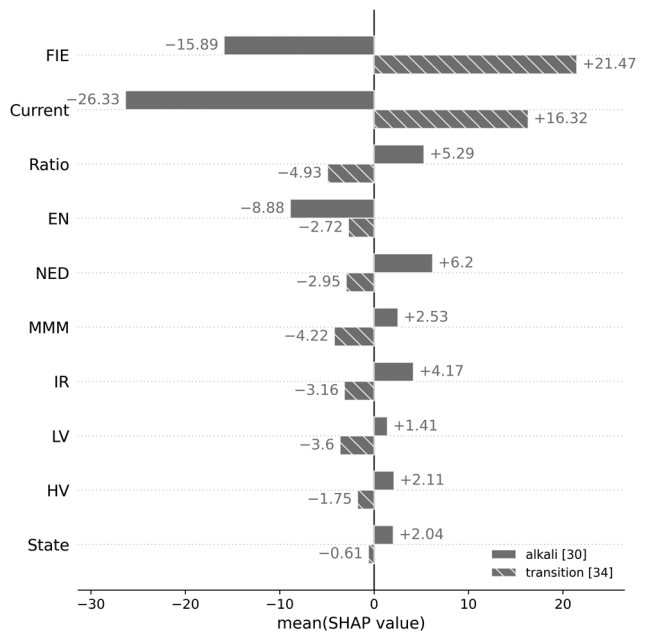

Fig. 5 Summary plot of mean SHAP values by feature and element type.

transition samples, FIE tends to increase the predicted DC. Other features like ratio, NED, MMM, IR, LV, HV, and state also contribute notably, though their direction and magnitude vary between element types. This cohort analysis helps in understanding both the magnitude and direction of each feature's contribution, as well as how these effects differ across chemical categories.

4. Challenges and future directions

The performance of MLMs is directly related to the structure of datasets to accurately predict the DC. The size and distribution of the data can help to determine the most suitable MLMs for training and testing, and the results will vary based on the dataset. To achieve optimal ML performance, it is important to maintain consistent conditions during data collection. In our present study, we have experienced the following difficulties in acquiring our dataset:

- The electrolyte is to be considered as the bridge between the anode and the cathode. So, in our data collection, we did not consider any information related to the electrolytes. Different electrolytes can make a significant change in the battery performance.
- Some anode materials were not similar. The performance of the anode material can also change the DC.
- The ratio of the conductive additive and binder in the preparation of the electrode can cause a significant change in the battery performance. Therefore, in our current study, accurately reporting these issues remains a challenge.
- We have also not categorized data relative to the phase of MnO_2, and even though the cathode material is fixed, it is still challenging to fully report the particle size associated with the cathode material.
- The current collector or substrate is not similar for all the cells.
- At present, no external datasets match our specific feature definitions and experimental protocols. Although our internal validation approach is rigorous and supports confidence in the results, validation using independent datasets in future studies will be essential to confirm and further strengthen the generalizability of our method.

In the implications of MLMs to datasets, it is essential to consider the same environment to collect data. Most of the time, it is very difficult to find common features from different papers. So, to resolve this problem in collecting the data, multiple experiments can be conducted in the same environment and under the same conditions.

5. Conclusions

In this study, we have considered the results of 57 published papers and have applied different filtering conditions to collect a dataset which contains 25 dopants. For each dopant, we have collected 11 different features in which six features are related to publication results and five features are related to the elemental properties of dopants. From the PCM, we have observed that the electronegativity of the dopant can increase the DC of MnO_2. So, the dopant which has a higher electronegativity can be considered to improve the performance of the MnO_2 cathode for ZIBs. Similarly, the DC of the MnO_2 cathode enhances with FIE of the dopant. We have also applied both classification and regression treatment to our dataset by considering different MLMs. It is observed that the RF model can classify DC with an accuracy of 0.72 within three predefined grades. From our regression treatment, it is found that the XGBoost model predicts DC with an R^2 value of 0.92, indicating that this model effectively captures the underlying variance in the data and yields a strong agreement between the predicted and actual DC values. So, this MLM can be considered to predict the performance of MnO_2 in ZIBs. The SHAP summary indicates that current, FIE, ratio, and MMM are the most influential features in optimizing the performance of the MnO_2 cathode. We also conducted a cohort analysis based on alkali and transition metal groups to examine feature importance and observed that these two groups generally exhibit inverse effects on the model's predictions. Therefore, the findings of this study can assist researchers in predicting MnO_2 performance based on various dopant characteristics before proceeding with laboratory synthesis.

Author contributions

Nure Alam Chowdhury: conceptualization, data collection, machine learning, writing – original draft, and review and editing. Leaford N. Henderson: conceptualization, data collection, and review and editing. Samin Yaser: machine learning. Olusola P. Oyeku: data collection. Maydenee M. Tresa: data collection. Chandra Kundu: machine learning, and review and editing. Jayan Thomas: conceptualization, review and editing, and supervision.

Conflicts of interest

There are no conflicts to declare.

Data availability

The data supporting this article have been included as part of the ESI.† The dataset and code for this article can be found at the following GitHub link: **https://tinyurl.com/396jsa4t**.

Acknowledgements

The authors acknowledge the University of Central Florida Office of Research for financial support. They also acknowledge the use of OpenAI's ChatGPT for assistance with language editing during the preparation of this manuscript. The authors are grateful to the anonymous reviewers for their constructive suggestions which have significantly improved the quality of our manuscript.

References

1 X. Hu, Y. Wang, X. Feng, L. Wang, M. Ouyang and Q. Zhang, *Renew. Sustainable Energy Rev.*, 2025, **207**, 114949.
2 G. Ji, L. He, T. Wu and G. Cui, *Appl. Energy*, 2025, **377**, 124538.
3 P. Wu, E. Tian, H. Tao and Y. Chen, *Eng. Appl. Artif. Intell.*, 2025, **141**, 109756.
4 J. Peng, Y. Chen, Y. Huyan, N. Li and J.-G. Wang, *Appl. Surf. Sci.*, 2023, **623**, 157060.
5 M. Song, H. Tan, D. Chao and H. J. Fan, *Adv. Funct. Mater.*, 2018, **28**, 1802564.
6 J. Wei, P. Zhang, J. Sun, Y. Liu, F. Li, H. Xu, R. Ye, Z. Tie, L. Sun and Z. Jin, *Chem. Soc. Rev.*, 2024, **53**, 10335–10369.
7 Y. Ren, S. Zhang, B. Yin, J. R. Loh, Y. Ding, X. Huang, J. Li, H. Li and T. Ma, *Batter. Supercaps*, 2023, **6**, e202300132.
8 Z. Ni, X. Liang, L. Zhao, H. Zhao, B. Ge and W. Li, *Solid State Ion.*, 2022, **386**, 116049.
9 J. Tan, T. Feng, S. Hu, Y. Liang, S. Zhang, Z. Xu, H. Zhou and M. Wu, *Appl. Surf. Sci.*, 2022, **604**, 154578.
10 L. Suo, O. Borodin, T. Gao, M. Olguin, J. Ho, X. Fan, C. Luo, C. Wang and K. Xu, *Science*, 2015, **350**, 938–943.
11 H. Xu, W. Yang, M. Li, H. Liu, S. Gong, F. Zhao, C. Li, J. Qi, H. Wang, W. Peng and J. Liu, *Small*, 2024, **20**, 2310972.
12 G. Li, L. Sun, S. Zhang, C. Zhang, H. Jin, K. Davey, G. Liang, S. Liu, J. Mao and Z. Guo, *Adv. Funct. Mater.*, 2024, **34**, 2301291.
13 A. Konarov, N. Voronina, J. H. Jo, Z. Bakenov, Y.-K. Sun and S.-T. Myung, *ACS Energy Lett.*, 2018, **3**, 2620–2640.
14 T. Li, N. Zhang, B. Liu, P. Wang, Z. Liu, Y. Wang, D. Xu, H. Tian, Q. Zhang and T. Yi, *Adv. Funct. Mater.*, 2025, 2423755.
15 G. Li, W. Yu, Q. Diao, Y. Zhang, F. Tang, X. Luo, L. Yan, X. Zhao and G. Li, *ChemPhysChem*, 2025, **26**, e202400860.
16 J. Wang, X. Sun, H. Zhao, L. Xu, J. Xia, M. Luo, Y. Yang and Y. Du, *J. Phys. Chem. C*, 2019, **123**, 22735–22741.
17 R. Lan, E. Gkanas, A. J. S. Sahib, A. Greszta, R. Bhagat and A. Roberts, *J. Alloys Compd.*, 2024, **992**, 174528.
18 D. Yan, H. Li, A. Yang, M. Wang, K. Nie, X. Lv and J. Deng, *Chem. Eng. J.*, 2025, **504**, 158966.
19 W. Qian, Z. Chen, L. Chen, Q. Sun, H. Zhou, Z. Zhou, H. Yang and J. Huang, *Appl. Surf. Sci.*, 2025, **684**, 161981.
20 R. Sinha, X. Xie, Y. Yang, Y. Li, Y. Xue, P. Wang and Z. Li, *Adv. Energy Mater.*, 2025, 2404815.
21 H. Fu, X. Wang, L. Ye, Z. Wu, J. Yang, M. Shi and E. H. Ang, *Chem. Eng. J.*, 2025, **506**, 160308.
22 Y. Qian, G. Chang, C. Huang, Y. Yang, Y. Hao, Q. Tang, A. Hu, Y. Li and X. Chen, *Chem. Eng. J.*, 2025, **503**, 158392.
23 H. Zhao, Y. Hao, Y. Zhang and Y. Gu, *J. Power Sources*, 2025, **630**, 236075.
24 X. Gao, H. Wu, W. Li, Y. Tian, Y. Zhang, H. Wu, L. Yang, G. Zou, H. Hou and X. Ji, *Small*, 2020, **16**, 1905842.
25 M. Liu, Q. Zhao, H. Liu, J. Yang, X. Chen, L. Yang, Y. Cui, W. Huang, W. Zhao, A. Song, Y. Wang, S. Ding, Y. Song, G. Qian, H. Chen and F. Pan, *Nano Energy*, 2019, **64**, 103942.
26 C. Wang, Y. Zeng, X. Xiao, S. Wu, G. Zhong, K. Xu, Z. Wei, W. Su and X. Lu, *J. Energy Chem.*, 2020, **43**, 182–187.
27 W. Zhao, Q. Kong, X. Wu, X. An, J. Zhang, X. Liu and W. Yao, *Appl. Surf. Sci.*, 2022, **605**, 154685.
28 Z. Tang, W. Chen, Z. Lyu and Q. Chen, *Energy Mater. Adv.*, 2022, **2022**, 9765710.
29 L. Liu, Y. Wu, L. Huang, K. Liu, B. Duployer, P. Rozier, P. Taberna and P. Simon, *Adv. Energy Mater.*, 2021, **11**, 2101287.
30 A. Zhang, X. Yin, X. Zhang, J. Ba, J. Li, Y. Wei and Y. Wang, *ACS Appl. Energy Mater.*, 2024, **7**, 1298–1305.
31 Z. Wang, K. Han, Q. Wan, Y. Fang, X. Qu and P. Li, *ACS Appl. Mater. Interfaces*, 2023, **15**, 859–869.
32 P. Lakhera, V. Chaudhary, A. Jha, R. Singh, P. Kush and P. Kumar, *Mater. Today Chem.*, 2022, **26**, 101129.
33 E. Moore, *Metal-Ligand Bonding*, Royal Society of Chemistry, Cambridge, 2004.
34 J. Heo, S. Chong, S. Kim, R. Kim, K. Shin, J. Kim and H. Kim, *Batter. Supercaps*, 2021, **4**, 1881–1888.
35 S. Chen, Y. Kong, C. Tang, N. A. Gadelhak, A. K. Nanjundan, A. Du, C. Yu and X. Huang, *Small*, 2024, **20**, 2312229.
36 Y. Liu, W. Chen, X. Zhao and X. Pan, *J. Alloys Compd.*, 2025, **1014**, 178725.
37 Y. Zhao, S. Zhang, Y. Zhang, J. Liang, L. Ren, H. J. Fan, W. Liu and X. Sun, *Energy Environ. Sci.*, 2024, **17**, 1279–1290.
38 Q. Li, C. Wang, Y. Zhu, W. Du, W. Liu, M. Yao, Y. Wang, Y. Qian and S. Feng, *Chem. Eng. J.*, 2024, **485**, 150077.
39 A. C. Müller and S. Guido, *Introduction to machine learning with Python: a guide for data scientists*, O'Reilly Media, Inc., Sebastopol, CA, 1st edn, 2016.
40 A. Géron, *Hands-on machine learning with Scikit-Learn, Keras and TensorFlow: concepts, tools, and techniques to build intelligent systems*, O'Reilly Media, Inc., Beijing, 3rd edn, 2023.
41 M. Mohri, A. Rostamizadeh and A. Talwalkar, *Foundations of machine learning*, MIT Press, Cambridge, MA, 2nd edn, 2018.
42 Z. Wei, Q. He and Y. Zhao, *J. Power Sources*, 2022, **549**, 232125.
43 Z. Nozarijouybari and H. K. Fathy, *J. Power Sources*, 2024, **601**, 234272.
44 M. Berecibar, *Nature*, 2019, **568**, 325–326.
45 K. A. Severson, P. M. Attia, N. Jin, N. Perkins, B. Jiang, Z. Yang, M. H. Chen, M. Aykol, P. K. Herring, D. Fraggedakis, M. Z. Bazant, S. J. Harris, W. C. Chueh and R. D. Braatz, *Nat. Energy*, 2019, **4**, 383–391.
46 Z. Wang, X. Lin, Y. Han, J. Cai, S. Wu, X. Yu and J. Li, *Nano Energy*, 2021, **89**, 106337.
47 G. Wang, T. Fearn, T. Wang and K.-L. Choy, *Energy Technol.*, 2021, **9**, 2100053.
48 G. Wang, T. Fearn, T. Wang and K.-L. Choy, *ACS Cent. Sci.*, 2021, **7**, 1551–1560.
49 Z. Wang, Y. Gu, L. Zheng, J. Hou, H. Zheng, S. Sun and L. Wang, *Adv. Mater.*, 2022, **34**, 2106776.
50 S. Ghosh, G. R. Rao and T. Thomas, *Energy Storage Mater.*, 2021, **40**, 426–438.
51 M. Jiang, Y. Zhang, Z. Yang, H. Li, J. Li, J. Li, T. Lu, C. Wang, G. Yang and L. Pan, *Inorg. Chem. Front.*, 2023, **10**, 6646–6654.
52 K. Das, R. Kumar and A. Krishna, *Renew. Sustainable Energy Rev.*, 2024, **189**, 113967.

53 Z. Jin, X. Li, Z. Qiu, F. Li, E. Kong and B. Li, *Energy*, 2025, **314**, 134229.
54 S. Liu, J. Chen, C. Zhang, L. Jin and Q. Yang, *J. Energy Storage*, 2022, **45**, 103418.
55 C. Zuo, F. Xiong, Y. Shao, M. Li, D. Zhu, J. Zhu, J. Wang and Q. An, *Energy Storage Mater.*, 2024, **72**, 103763.
56 S. Watanabe, *arXiv*, 2023, preprint, arXiv:2304.11127, DOI: **10.48550/arXiv.2304.11127**.
57 S. M. Lundberg, G. G. Erion and S.-I. Lee, *arXiv*, 2019, preprint, arXiv:1802.03888, DOI: **10.48550/arXiv.1802.03888**.
58 S. Lundberg and S.-I. Lee, *arXiv*, 2017, preprint, arXiv:1705.07874, DOI: **10.48550/arXiv.1705.07874**.
59 D. Janzing, L. Minorics and P. Blöbaum, *arXiv*, 2019, preprint, arXiv:1910.13413, DOI: **10.48550/arXiv.1910.13413**.
60 K. Aas, M. Jullum and A. Løland, *Artif. Intell.*, 2021, **298**, 103502.